Direct and indirect measurement of rain drop size distributions using an acoustic water tank disdrometer

2013 Meas. Sci. Technol. 24 065801

(http://iopscience.iop.org/0957-0233/24/6/065801)

Meas. Sci. Technol. **24** (2013) 065801 (11pp) doi:10.1088/0957-0233/24/6/065801

Direct and indirect measurement of rain drop size distributions using an acoustic water tank disdrometer

P N Winder[1] **and K S Paulson**

Department of Engineering, University of Hull, Hull HU6 7RX, UK

E-mail: philipwinder@gmail.com

Received 16 October 2012, in final form 9 March 2013
Published 19 April 2013
Online at stacks.iop.org/MST/24/065801

Abstract
Several rain drop size distribution (DSD) point measurement technologies exist, but all are unable to sample either short timescales or the large drop tail of the DSD due to inherent instrumental limitations. The development of an acoustic water tank disdrometer (AWTD) is described, which improves the sampling statistics by increasing the catchment area. This is achieved by distinguishing individual drops, locating them on the surface of the tank then converting the impact pressure into a drop size. Wavelet decomposition is used to distinguish the broadband, short duration impact events and a fast multilateration method is used to position the drop. Issues relating to the different types of noise are also investigated and mitigated. Also, further work on inverting the measured acoustic intensity into a DSD, by fitting sampling distributions, is presented. Six months of data were collected in the Eastern UK. The AWTD then converted the data into DSDs and the results were compared to a commercially available co-located laser precipitation monitor. The sampling errors are far lower due to the increased catchment size, and hence the large drop sized tail of the DSD is greatly improved. DSD results compare favourably to other disdrometers for drop diameters greater than 1.8 mm. Below this size individual drops become increasingly difficult to detect and are underestimated.

Keywords: disdrometer, rain, gauge, acoustic, water, tank, atmospheric, DSD, raindrop, drop, size, distribution, AWTD, entrainment, multilateration, impact

(Some figures may appear in colour only in the online journal)

1. Introduction

The rain drop size distribution (DSD) is a measurement that counts the number of drops in a particular size bin then collates their frequencies into a distribution. Several point DSD measurement technologies exist and can be categorized by describing the way they interpret the rain event: energy conversion, scattering and observational. Some examples are the Joss–Waldvogel impact disdrometer (Joss and Waldvogel 1967), the Thies Clima laser precipitation monitor (LPM) and the two-dimensional video disdrometer (Kruger and Krajewski 2002), respectively. These instruments attempt to measure the size of the drop as they fall through or onto a horizontal catchment area directly, or through an empirical relationship. The near simultaneous arrival of two or more drops leads to erroneous measurements so each technology mitigates this by using a limited catchment area, which has been shown to severely limit the temporal statistics of the measured data; i.e. the integration time must be long in order to better sample the large drop size tail of the DSD (Winder and Paulson 2012).

The detailing of the sub-second variation in the large drop size tail of the DSD is particularly important in some applications, for example in soil erosion and radio communications. In radio communications the scattering from a raindrop is proportional to its diameter raised to the sixth power. Hence radar reflectivity and microwave specific

[1] Author to whom any correspondence should be addressed.

attenuation are very sensitive to the numbers of large drops (COST 210 1991). Similarly, erosion processes are highly non-linear with respect to drop size (Dijk *et al* 2002). Erosivity is a combined function of the rain intensity and of the drop velocity spectrum, so rain kinetic energy flux is often cited as a primary indicator, e.g. Brodie and Rosewell (2007) and Salles and Poesen (2000). A large proportion of the kinetic energy is carried by the small proportion of larger drops.

A relatively new form of impact disdrometer uses a body of water as the catchment and deduces rain parameters from analysis of the acoustic signals generated by impacting drops e.g. Nystuen (1987), Oguz and Prosperetti (1991), Nystuen *et al* (1993), Nystuen (2001), Ma *et al* (2005) and Winder and Paulson (2012). Early efforts concentrated on establishing a relationship between the acoustic intensity and the rainfall intensity (the volume of rain arriving at a horizontal unit catchment area per unit time). Nystuen *et al* (1993) found usable correlations between rainfall intensity and the power in parts of the acoustic frequency spectrum. Later, the technique was improved to provide correlation coefficients of between 0.84 and 0.9 depending on the comparison instrument (Nystuen 2001). However, this algorithm uses conditional corrections, based on empirical observations of the spectra, to compensate for the disproportionately loud impacts of larger drops and the loud and long duration noise signal produced by the oscillation of entrained bubbles. The possibility of very short integration time rainfall intensity estimates is one of the motivations for this paper. Nystuen and Amitai (2003) report rainfall intensity time-series with 5 s resolution (integration time), yielding rainfall intensities up to an event maximum of 1600 mm h^{-1}. These extreme values are not recorded by the other types of rain gauges due to the requirement of much longer integration times.

There is also the possibility to invert the measured acoustic field to estimate the DSD. The system of Nystuen (2001) is constrained by the filtering of noise. Therefore the system can distinguish drop diameters in only four, or sometimes two (for low rain intensities) size ranges. This is clearly inadequate to produce a description of arbitrary DSDs but may be sufficient to estimate the parameters of an exponential or gamma distribution.

A more recent proposal is the inversion of the signal generated by individual drop impacts to yield individual drop size, and to hence build a DSD. The acoustic signal generated directly by a drop impact is very short, approximately 40 μs, and so the possibility exists to use a large catchment area and to measure many impacts in a short time. However, great difficulties are introduced by other noise sources, principally the sounds produced by entrained bubbles. Many experiments have already established the processes leading to sound production by drop impacts, e.g. Franz (1959), Pumphrey and Crum (1989), Medwin *et al* (1990), Manzello and Yang (2002) and Prosperetti and Oguz (1993). These have shown that an impacting drop produces several different signals, including transients upon raindrop impact and exponentially decaying sinusoids due to oscillation of entrained bubbles. Further work has attempted to model this process (Guo and Williams 1991, Oguz and Prosperetti 1991) and others have used this information to create total sound profiles. The production of entrained bubbles depends upon many parameters such as drop size, impact speed and angle of incidence. The complicated physics behind these processes leads to non-linearities in the acoustic-rainfall intensity inversion process. Bubble noise also greatly complicates the estimation of DSD from the acoustic signal.

A previous paper (Winder and Paulson 2012) examined the use of an acoustic, water tank disdrometer (AWTD) as an estimator for rainfall intensity based from acoustic intensity measurements. The AWTD yielded rainfall intensity with a 1 s integration time and with a very high correlation to standard meteorological instrument with lower temporal resolution. This paper explores the measurement of the DSD indirectly, by the estimation of exponential and gamma DSD parameters; and directly, by automatically locating and quantifying the size of an impacting raindrop from an array of hydrophone measurements.

2. Hardware

The AWTD has several major components, each designed to maintain the required experimental flexibility. These include: a water tank, an anechoic lining, hydrophones with amplifiers, data acquisition hardware and a processing computer.

Four SRD Ltd HS-150 hydrophones were used to measure the acoustic signal. With a resonance at 150 kHz, the hydrophones have a flat working spectral region from 100 Hz to 100 kHz ($\pm$ 3 dB), omnidirectional to 280° ($\pm$ 1 dB) and a sensitivity of $-$204 dBV re. 1 μPa. An experimental calibration was performed by measuring the received amplitude from a known distance. A multiplier is then applied in the software to compensate for the variation in sensitivity.

A tank of water is used to provide a consistent surface for raindrops to impact upon. A cylindrical plastic high density polyethylene tank with an outer radius of 0.4 m, an inner radius of 0.35 m (after adding the anechoic lining) and a depth of 0.59 m, was chosen because of its wide availability, low cost and appropriate size. Ultimately, the size of the tank is limited by the sensitivity of the hydrophones and the associated electronics. This sets a limit on the size of drop that can be detected.

An impacting drop produces an impact signal that would be received at the four hydrophones at varying times. Since the speed of sound in the water is consistent and the hydrophone placement is known, the time of arrivals of the impact signal can be used to locate the position of the source drop.

The data acquisition card is a National Instruments PCI-4462 with a maximum sampling rate of 200 kS s^{-1} at a resolution of 24 bits. Most importantly, it has four simultaneously sampled inputs and onboard anti-aliasing filters.

Amplification was necessary to increase the amplitude of the hydrophone output, of the order of nanovolts, to a level above the noise floor of the data acquisition quantization. A bespoke charge amplifier with a significant amount of power supply filtering was designed, using the high input impedance and low voltage and current noise AD8066 operational

Figure 1. The AWTD co-located with the LPM and anemometer in the field. The wires down the side of the tank are the hydrophone cables. The semi-anechoic lining covers all interior surfaces of the tank. Further foam covers the outside to prevent signals being generated by drops impacting on the outer tank surface.

amplifier. The noise floor of the combined hydrophone, amplifier and data acquisition was experimentally measured to be approximately 700 μV RMS, or equivalently to an acoustic signal of 0.1 Pa (according to the hydrophone datasheet). This figure seems high, but is including the noise from all components of the AWTD. For example, the switching power unit within a computer will be adding a significant amount of noise to the data acquisition. The PCI data acquisition card, connected to the amplifier and the hydrophones, was fitted into a standard office PC.

To reduce reflections that could be misinterpreted as an impact, an absorptive lining was constructed of out a combination of natural rubber backed with an open cell foam. This lining was approximately a hundred times cheaper than any commercially available solution. The natural rubber has a density that is very similar to that of water, which reduces reflections at the lining surface, and is also very lossy, absorbing the sound during propagation. The open cell foam also provides some attenuation due to its structure and combines with the rubber to produce a cavity that is semi-resonant at approximately 50 kHz. This provides a significant amount of damping. The lining yields a combined loss factor of 0.1 (measured by itself, not in the AWTD) which is approximately that predicted by the model of Ouis (2005) (0.1–0.125). Further foam was wrapped around the outside of the tank to prevent raindrops impacting on the outside walls causing a sound inside the tank.

Figure 1 is a photograph of the instrument in the field, collocated with a Theis LPM and a sonic anemometer.

3. Direct interpretation methodology

The major objective of this project was to use the AWTD to identify each impacting drop and to estimate its size. The DSD can then be generated when sufficient drops have been detected. This would not assume any particular form for the DSD. Instead, the atmospheric concentration of drops in diameter ranges would be calculated from their rate of impact on the tank surface. This process relies upon the existence of a direct link between the measured impact acoustic signal and the drop diameter. However, as we have seen earlier, the acoustic signal has stochastic components and will experience different propagation fading and distortion depending on the impact location.

Research on the impact pulse produced by a drop impact provides experimental results that show that the amplitude is related to the impacting drop's size and velocity. Pumphrey and Crum (1989) reported that 'the true initial impact pressure is proportional to the impact velocity to a power between 2.5 and 3'. This result supports the work of Franz (1959) who suggests that the pressure is proportional to the velocity cubed. Furthermore, the impact pressure was also stated as proportional to the drop diameter to a power of 2.1 $\pm$ 0.6, assuming that each drop is travelling at its terminal velocity. Therefore, if the impact pulse can be separated from the associated entrained bubble noise, and drops can be assumed to be falling at their terminal velocity, drop diameters can be estimated from the impact pulse amplitude.

3.1. Noise

The damped sinusoidal acoustic signal produced from trapped air bubbles provides the greatest problem in acoustic disdrometry. Bubble signals have little relation to the parameters of the impacting drop that generated them, do not occur on every impact event, and could have been produced by one of three mutually exclusive mechanisms (Prosperetti and Oguz 1993). Also, when the bubble signal is produced, it is often significantly larger in amplitude than any corresponding impact signal. The coincidence of bubble and impact signals makes drop parameter estimation considerably more difficult.

It has been shown that bubbles could be suppressed by reducing the surface tension of the liquid in the tank (Pumphrey and Crum 1989). More recent work investigated how the surface tension can affect entrainment (Deng *et al* 2007). The viscous effects of the liquid had been neglected in most previous studies, but both studies found that the size of the entrainment bubble tends to be proportional to surface tension and inversely proportional to viscosity. This is partly due to both viscous damping, which decreases the angle of the crater cone, and by the surface tension, which limits the crater's ability to pinch-off (i.e. collapse). By adding a food-oil layer to the top of the water tank it was possible to create a highly viscous cushion for the impact, which limited crater formation. Without a crater, entrainment could not occur, thus removing all sources of entrainment noise. However, using an oil covered surface is not practical in a rain measurement instrument. Oils are not stable over time and tend to harbour organic growth. There is also the problem of water puddles forming on the oil surface, which change the impact signal and can cause entrainment. An alternative to increasing viscosity is the reduction of surface tension by the addition of a soap based surfactant. This does reduce entrainment but leads to the production of surface bubbles that generate high amplitude impact-like signals when they burst. In heavy rain a surface foam was formed which also affected the impact signal.

A successful method of removing the entrainment noise is by positively identifying impacts. Simple notch or high-pass filters are unusable since bubbles and impacts contain similar frequency components (Medwin *et al* 1992). Wavelet decomposition, using a discrete Meyer function, was found to be better suited to impact pulse filtering than other methodologies. Wavelet decomposition was chosen because a high temporal resolution was required for subsequent location routines. The discrete Meyer wavelet was chosen due to a high correlation coefficient between an impact pulse and the wavelet. An interested reader can find further details in Winder (2010).

Other sources of noise include electrical and wind; creating waves, moving the cables, and flexing the water tank. Electrical noise was suppressed with inductive-capacitive filters on the power lines and by properly grounding the cable's outer sheath. The cables were lightly buried to avoid cable movement. Waves were not seen, since the AWTD's body of water is small and wind speeds are generally low due to vegetation shielding around the AWTD site. However, the high density polyethylene walled tank is fairly thin, approximately 1–2 mm, and does not provide the structural rigidity to hold the tank in place during high winds. From experimentation, the wind signal has frequency components up to 1 kHz which depend on wind speeds and resonances of the tank structure. A high pass filter with a cut-off frequency of 1 kHz adequately filters any remaining mains and wind noise.

3.2. Further processing

After thresholding the filtered data, a set of four impact impulses are required for localization and drop sizing and are often mixed with the impulses from other drops. Further processing is required to decode the mixed sets of impulses. This involves using physical limits such as the tank size and logical rules like 'there can only be one impulse on each hydrophone' to ascertain the correct impact dataset. Further details can be found in Winder (2010).

3.3. Multilateration

The process of multilateration is used to localize the drop (within the tank) and estimate the range to normalize the impact impulse pressures. It may be written as a solution of coupled, multivariate, nonlinear equations. Assuming the impact occurs at time zero and using Pythagoras' theorem, it is possible to calculate the time of arrival from a source at x, y and z by

$$\mathrm{TOA}_n = \frac{1}{c}\sqrt{(x-x_n)^2 + (y-y_n)^2 + (z-z_n)^2}, \qquad (1)$$

where n is the hydrophone number and takes the value of $n = 1 \ldots N$, N is the number of hydrophones, x_n, y_n and z_n give the location of the nth hydrophone and c is the speed of sound in the medium. For this application, z and z_n are the known depth of the tank. The TDOA pairs can be calculated as

$$\begin{aligned} \mathrm{TDOA}_{13} &= \mathrm{TOA}_3 - \mathrm{TOA}_1 \\ \mathrm{TDOA}_{24} &= \mathrm{TOA}_4 - \mathrm{TOA}_2. \end{aligned} \qquad (2)$$

3.3.1. Simplification and solution. Using the symmetry of two vertical pairs of hydrophones, equations (1) and (2) can be simplified considerably. Furthermore, as all parameters are bounded by the tank dimensions and the depth is fixed, the resultant can be computed efficiently using numerical methods. This also allows the use of a three hydrophone version to localize the position of an incomplete impact impulse dataset. The full derivation can be found in Winder (2010).

3.4. Drop size approximation

Several studies have attempted to form a model of the impact process with the aim of predicting the amplitude of the impact signal (for a review see Prosperetti and Oguz 1993). Oguz and Prosperetti (1991) constructed a model based upon the dipole nature of the radiated pressure, p, which was confirmed by Pumphrey and Elmore (1990). The resultant model is dimensionally correct, however the relative contributions of V and d have been shown experimentally to vary considerably. The model of Oguz and Prosperetti (1991) predicts the received impact amplitude pressure, p, to be

$$p \approx \frac{\cos(\theta)}{r}\frac{\rho V^3 d}{c} u\left(\frac{Vt}{d}\right) \qquad (3)$$

where θ and r are the azimuth angle and distance from the water plane to the listening device, ρ is the density of the water and u is a dimensionless function that describes the '*details of the process*' (Prosperetti and Oguz 1993). Beyond this, the link between drop parameters and the amplitude of the impact wave are less well known. Although a range of complex empirical expressions exist, (e.g. those of Pumphrey and Crum (1989) and Pumphrey (1991)), calibration would be necessary using the geometry, material and equipment of the AWTD. To test the validity of these models in the AWTD, drop size experiments were performed.

3.4.1. Size relationship. The aim of this experiment is to match the LPM size data to the pressure amplitude of the impact wave derived from the AWTD hydrophone data. A lid was placed over the AWTD with an aperture immediately below the LPM catchment and directly above one of the hydrophones. This fixes the distance travelled by a propagating impact wave to the depth of the tank (0.59 m) and only allows raindrops into the tank that have passed through the LPM catchment first. Foam was placed on the tank lid to prevent noise associated with drops missing the opening. Splashes were inherently ignored due to their slow velocity. A rain event was then artificially simulated using an elevated sprinkler. The wind speed around the AWTD site was monitored by placing an anemometer next to the AWTD. The vast majority of DSDs reported a wind speed of less than 1.5 m s^{-1} (see Winder 2010). The velocity uncertainty due to wind will be absorbed into the drop estimation error for the sake of simplicity.

3.4.2. Size relationship results. The resultant drops travelled a total vertical drop of approximately 8 m; the majority of small to medium drops would attain their terminal velocity. From the drop size, the expected terminal velocity was calculated. If the measured velocity of any drops that did match their terminal velocity estimates ($\pm$ 10%), they were excluded from the resulting dataset. Since there may have been many drops that were invalid, the process of aligning the LPM size data to the hydrophone data was not automated. Instead this task was performed manually when it was certain hydrophone impact spikes could not be confused. Hence, relatively small amounts of drop velocity and impact pressure data were produced. Normalizing the impact pressure amplitudes (since the impact location was fixed), the data and regression of figure 2 were produced. These data are consistent with a power-law linking impact pressure (at a 1 m reference distance), p_0, and drop size, d:

$$d = 4.1 \times p_0^{0.4}. \quad (4)$$

Equation (4) can now be used to calculate the drop size from the normalized impact pressure. It states that the impact pressure is proportional to the diameter raised to the power of 2.5. This value is higher than the estimates of Pumphrey and Crum (1989) (1.6–1.8) and Pumphrey (1991) (1.5 $\pm$ 0.2) but is within the bounds of Franz (1959) (2.1 $\pm$ 0.6). Further experimentation and better analysis would improve the reliability of this value.

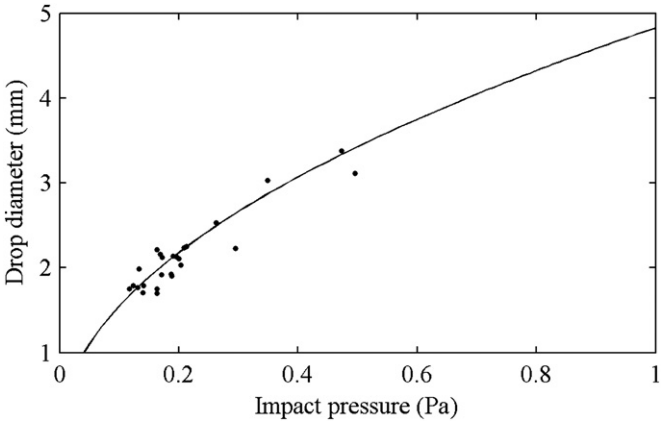

Figure 2. Results from the drop size-impact pressure experiment. Dots are individual drop sizes matched to their corresponding signal plotted with power law best fit curve.

3.5. Application

Each processed dataset is converted into a drop size. The drop impact position is calculated by multilateration and then the distance and azimuth angle to each hydrophone is calculated. This information is used to calculate the normalized pressure which is then calibrated using a multiplier obtained from a calibration experiment. Equation (4) is then used to calculate the drop diameter. The final diameter estimate is the average of the diameters calculated from each of the four hydrophones. Finally the drop diameter is saved into a DSD for later analysis.

4. DSD generation results

A cumulative total of 26.6 h of AWTD acoustic and LPM DSD rain data, collected over a period of six months, have been converted into minute long DSD distributions. The data collection period overlapped with the driest six months in the UK for 80 years. Section 4.1 first presents the results from using the acoustic intensity to indirectly estimate the DSD. Section 4.2 presents the results from direct observation of the DSD via the conversion process previously outlined in section 3.

4.1. Indirect interpretation of the DSD

A previous paper established a link between the acoustic intensity and rainfall intensity based upon a power law fit to a scatter plot of AWTD measured acoustic intensity and rainfall intensity determined from the LPM (Winder and Paulson 2012). It is also likely that there are other statistical links between the acoustic intensity and components of the DSD. A similar result has been achieved by Nystuen who uses several spectral parameters to formulate a simple DSD although the resolution of the DSD is poor (Nystuen 2001). Methods to estimate DSDs from the measured acoustic intensity are not only important to the AWTD but also to oceanic acoustic rain gauges, which often only estimate rainfall intensity and, at best, estimate DSD parameters according to Nystuen (2001).

When DSDs are averaged over a long period they can be described by a variety of standard size distributions. The

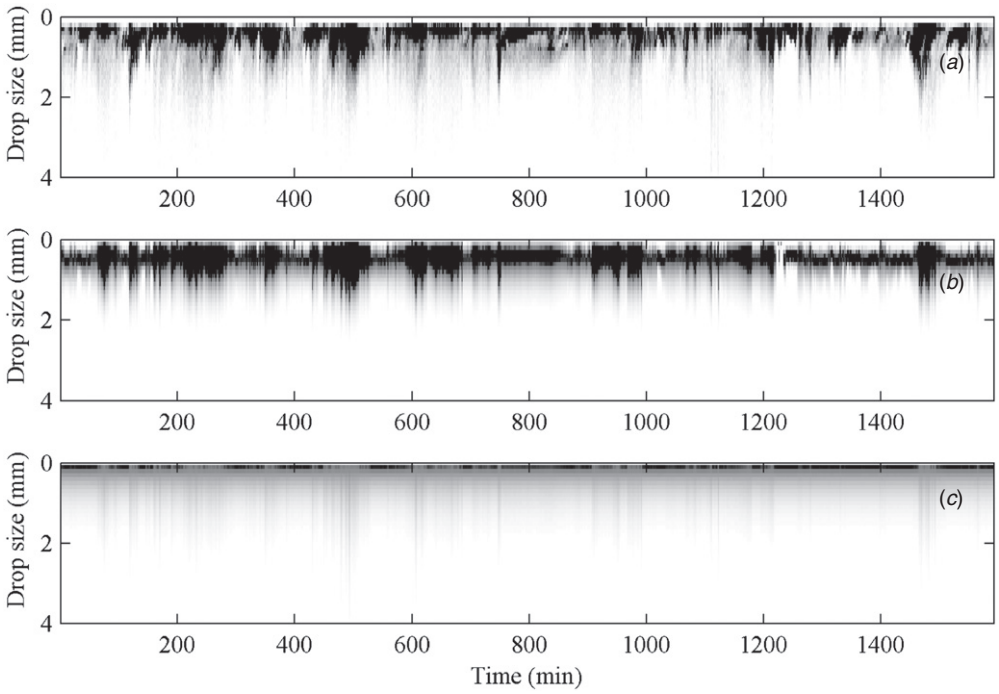

Figure 3. Temporal LPM DSD (*a*) data (*x*-axis = time, *y*-axis = drop size, *z*-axis = number of drops) can be compared to results from estimating gamma (*b*) and Marshall–Palmer (*c*) distributions from AWTD acoustic intensity data. The gamma based DSD estimation mirrors the LPM DSD well.

most cited is the Marshall-Palmer distribution which is based on an exponential distribution (Marshall and Palmer 1948). However, it was later found that the DSD is more accurately described by a gamma distribution (Ulbrich 1983). It is possible to represent the entire DSD by the shape parameters of the particular distribution: 1 for an exponential, 2 for a gamma, and a multiplying factor (scale) to account for the number of drops recorded.

After fitting exponential and gamma distributions to the LPM DSD data, the distribution parameters may then be compared to measurements of the acoustic signal. As in the previous paper, the total acoustic intensity was fitted to the parameters of the exponential and gamma distributions (a discussion of how a single power measurement can yield several parameters is discussed later). The acoustic intensity-parameter fits, which are based upon a series of linear and power law approximations, can be used to estimate 1 min gamma or Marshall–Palmer distributions, as seen in figure 3. The estimated gamma and Marshall–Palmer distributions plotted in (*b*) and (*c*), respectively can be compared to the LPM DSD in plot (*a*).

Several randomly selected examples of 1 min averaged LPM DSD data can be compared to the gamma and Marshall–Palmer estimates in figure 4.

The exponential fit, (*c*), overestimates the large drop tail of the DSD, underestimates the mid-size drops and overestimates the number of very small drops. The gamma fit, (*b*), fits the measured DSD well, with the effect of smoothing the DSD. This can be expected as a result of fitting an approximation. Local variations around the approximation are the largest source of error.

After averaging over all measured and gamma fitted DSDs (i.e. the average of all the DSD data in figure 3), the Pearson correlation coefficient is 0.90. Nystuen (2001) has found that correlation coefficients for standard commercial instruments yield between 0.79 and 0.94 which indicates that over a long period of time a total acoustic pressure-derived DSD could be as accurate as other disdrometers, although the instantaneous correlation is much lower. These results are easily explained by the general link between the rainfall intensity and the acoustic intensity found previously (Winder and Paulson 2012 and Nystuen 2001) and also that a DSD will tend towards a gamma distribution. The most interesting result is that the two shape parameters and the scale parameter for the gamma distribution were fitted only to linear and power laws of the acoustic intensity data (more details can be found in Winder 2010). This indicates that the parameters are not independent and hence three parameters may not be required for this level of accuracy. Future work could test this hypothesis by formulating a model that investigates this dependence. Also, the resultant correlation coefficient was generated using the same data that was used to fit the distribution parameters; further experiments should use independent training and test data sets to confirm the high correlation values.

4.2. Direct interpretation of the DSD

Figure 5 plots the average LPM DSD data against the average AWTD generated DSD data. Error bars (shading), representing the average standard error for each bin, are also plotted. It can be seen that the AWTD DSD approximates the LPM DSD well (a quantitative analysis will be presented later).

The benefits of the AWTD's large catchment area can be seen in the large drop tail of the derived DSD. Here the

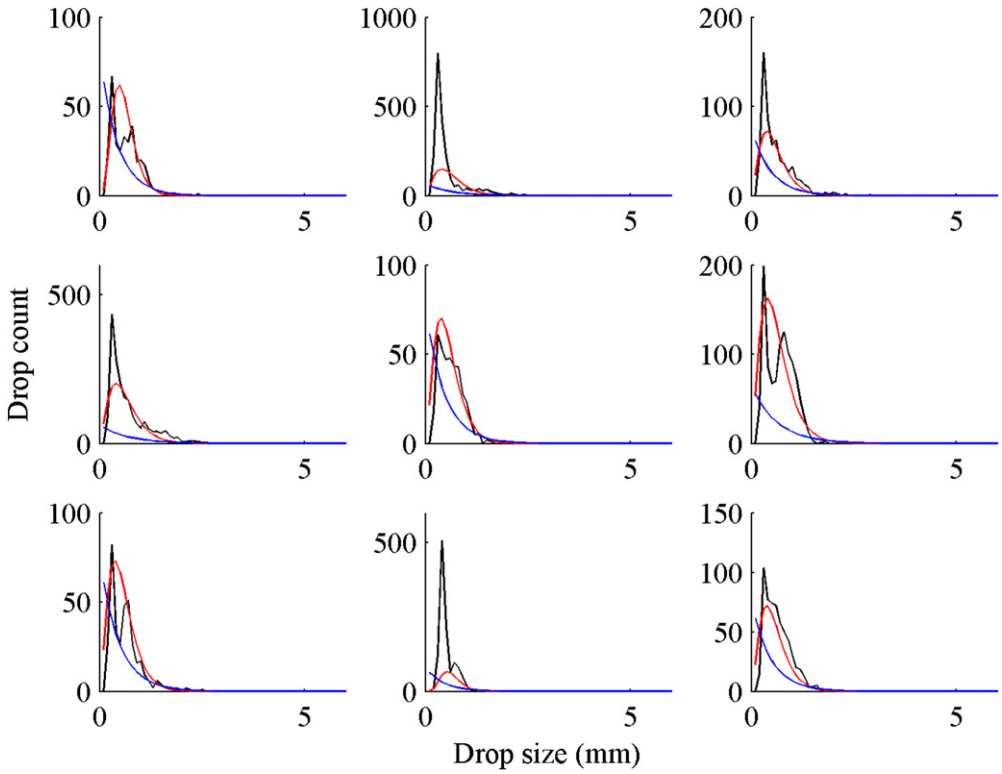

Figure 4. Randomly selected DSD examples from figure 3 where the LPM measured DSD is in black, the gamma distribution estimate is in red and the exponential distribution estimate is in blue.

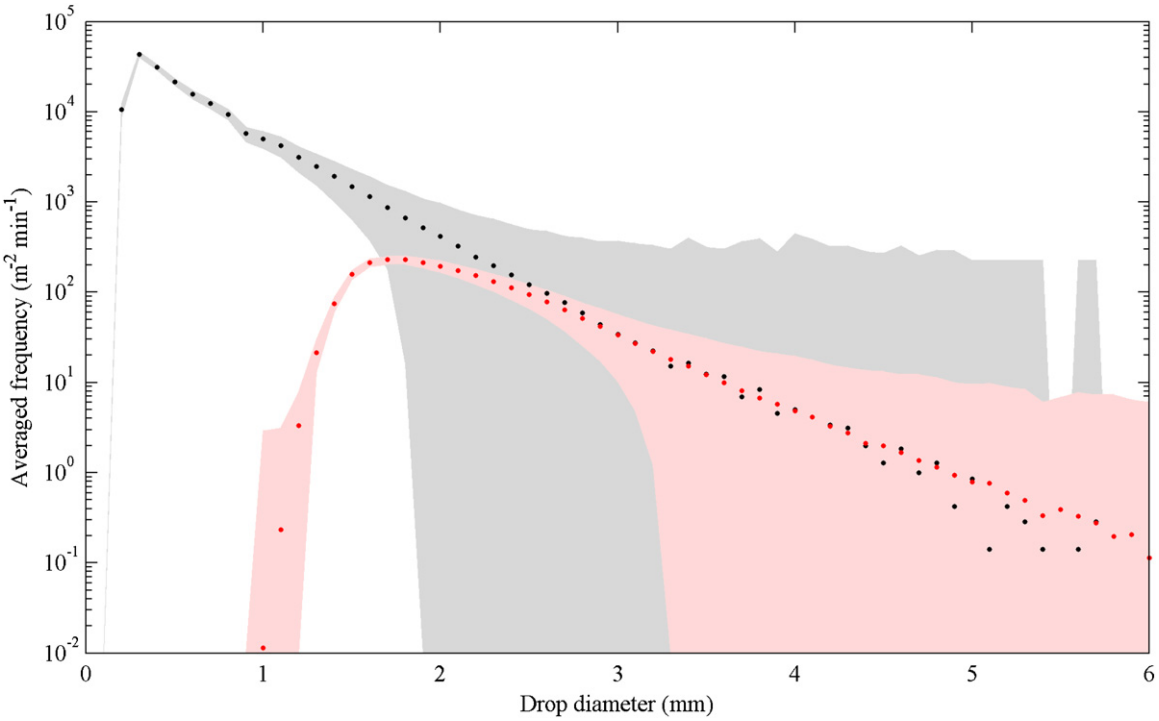

Figure 5. Averaged minute long DSD data from the LPM (black dots = mean, grey shading = standard error) and AWTD with a logarithmic *y*-scale (red dots = mean, light red shading = standard error). This plot emphasizes the improved accuracy of the AWTD at large drop sizes but also that it begins to underestimate the number of drops below 2.5 mm (although insignificant) and cannot detect drops below 1.8 mm in diameter (significant).

data are either highly uncertain or non-existent for the LPM, while the AWTD has measured sizable numbers of drops. A major feature of the AWTD is that the much larger catchment area provides much better estimates of the numbers of large drops. Alternatively, DSDs can be estimated with the same accuracy as with the LPM but for integration times a factor of

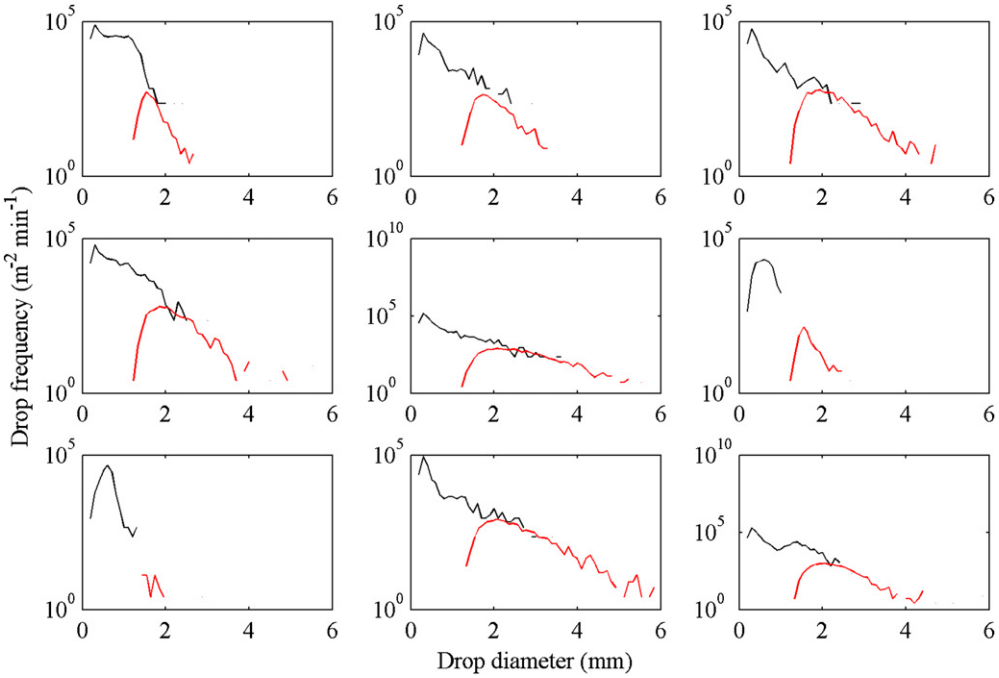

Figure 6. Randomly selected individual minute long DSDs for the LPM (black) and AWTD (red). Note the lack of LPM data at larger drop sizes. Ignoring the obvious difference in sampling characteristics (the AWTD cannot discern small drops, the LPM cannot discern large drops) the DSDs are agreeable. Another interpretation could find that the AWTD overestimates the size of the drops and underestimates their number caused by an incorrect pressure-drop size calibration. This is unlikely due to the calibration performed in section 3.4.4.

85 times shorter. The AWTD also significantly underestimates the number of drops below 1.8 mm. This is because the received impact pressure pulse is below the noise floor of the system.

4.2.1. Individual DSD examples. Several examples of the individual 1 min DSDs can be seen in figure 6. One can visually apply a hypothetical fit to find that even in the most extreme circumstances (i.e. the LPM does not see any large drops: e.g. the DSDs in the east and south-west positions), the results are largely agreeable.

4.2.2. Temporal DSD data. A plot of all the DSD results for both the AWTD and the LPM can be seen in the image plots of figure 7.

In figure 7 the plot of the LPM's DSD, (*a*), compared to the AWTD's DSD, (*b*), is not detailed enough to be able to accurately represent the large drop tail of the DSD. For example, consider the event at approximately 505 min. The LPM data describe the event as a fairly long (wide) event with a maximum drop size of approximately 3–4 mm. However, the AWTD shows that for a brief time within the event the maximum drop size increases dramatically to above 5 mm. This type of event could very easily prevent a communications link from operating and is not detected by the LPM. This is emphasized in figure 8, which is a plot of the total number of observed drops above 4 mm.

One discrepancy that severely degrades the temporal correlation is the error between 1065 and 1085 min in figures 7 and 8. The cause of this error is unknown and is open to speculation. The LPM data report uncharacteristically high frequencies of large drop sizes that the AWTD does not. It could be due to non-liquid hydrometeors. It could even be due to non-meteorological effects such as insects or animals (e.g. spiders spinning a web around the lens of the LPM) or simply, an error within either instrument.

4.2.3. Temporal analysis. The lack of comparative data makes a quantitative analysis difficult. One method of comparison is to fit an exponential (M-P) distribution to each minute long DSD. This yields scale and shape parameters that can be compared over time to provide a temporal correlation coefficient. A gamma distribution would better describe the atmospheric DSD over short timescales. However, for the purposes of comparison, the increased error is less important than the simplicity of single shape and scale parameters.

Figures 9 and 10 depict the shape and scale parameters of a maximum likelihood-fitted exponential distribution to each minute long DSD. A scale parameter for all drop diameters (i.e. including those less than 1.8 mm in diameter) is not generated since it is proportional to the number of observations, which is disproportionately underestimated by the AWTD (it cannot hear drops below 1.8 mm and potentially misses thousands of drops). It can be seen that the AWTD fits the LPMs shape parameter well and results in a Pearson correlation coefficient of 0.7. The scale parameter fits well with a Pearson correlation coefficient of 0.8. The erroneous event between 1065 and 1085 min can clearly be seen in the plot.

4.2.4. DSD Errors. The two most obvious differences between the AWTD and LPM DSD are within the smaller drops between 1 and 3 mm and the larger drops above 5 mm.

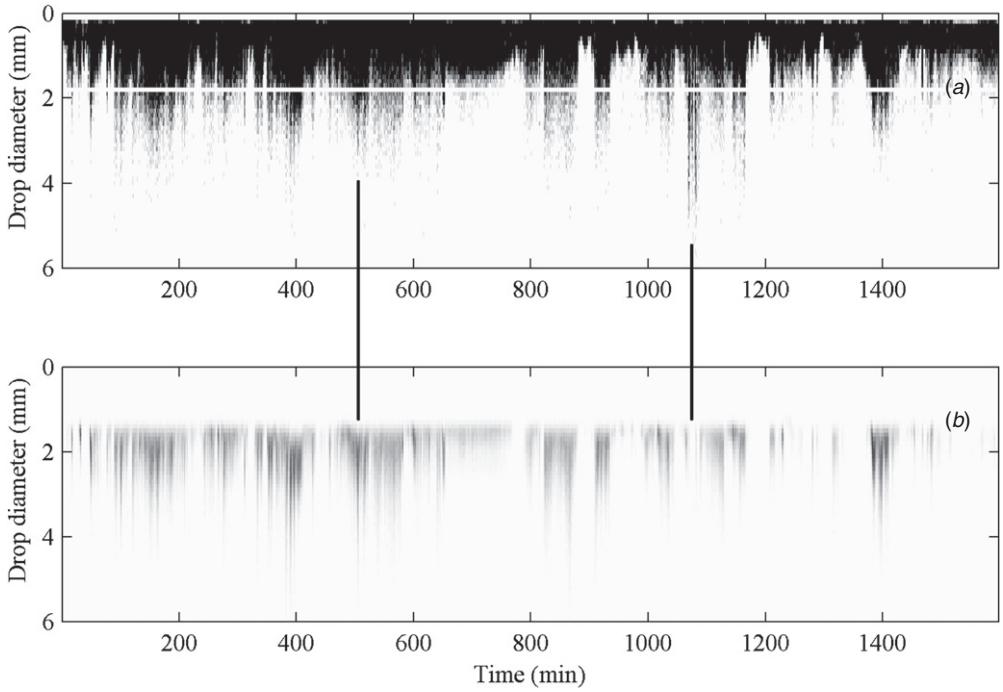

Figure 7. Minute long DSDs for all rainfall data for (*a*) the LPM and (*b*) the AWTD. The white line in the LPM data is the minimum discernible drop size of the AWTD (1.8 mm). The two black lines are markers for discussion.

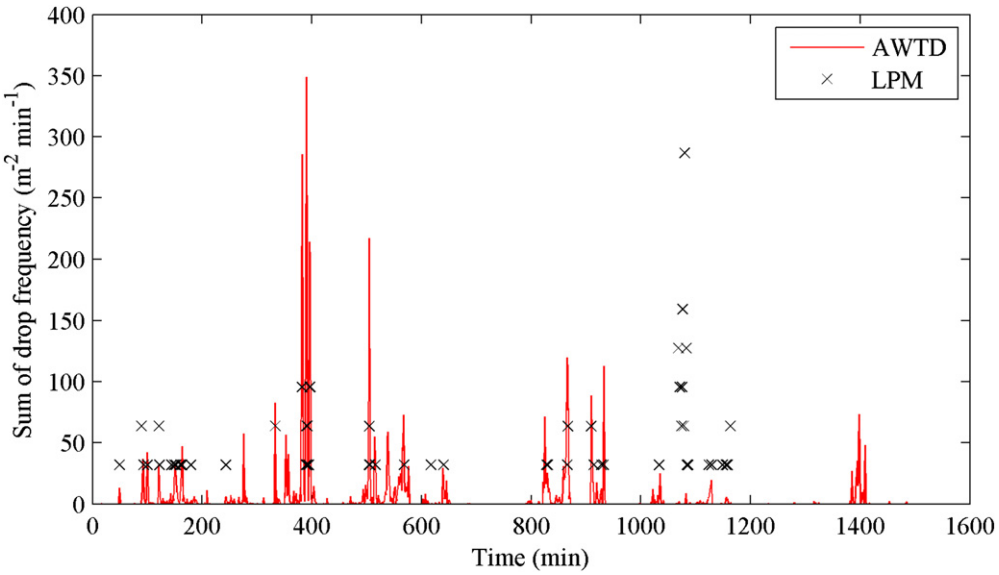

Figure 8. A plot of the total number of observed drops above 4 mm. The LPM data are plotted as black crosses (to emphasize the quantization) and AWTD data are in red. Note the difference in resolution and the disagreement at 1075 min.

Below a diameter of approximately 2.5 mm the drop impacts become increasingly difficult to distinguish from noise and drops are missed. This happens over a range of drop sizes due to the location of the impacting drop. Above diameters of approximately 3 mm all hydrophones can hear an impact, irrespective of where the impact occurs in the tank. However, for the purposes of DSD generation, the smallest discernible drop is taken at the point where the AWTD DSD begins to tend towards the LPM DSD, at 1.8 mm.

Above 4 mm, the AWTD appears to measure more large drops than the LPM DSD. The atmospheric sampling statistics are very poor for these drop bins. The LPM has measured a total of only a few tens of these drops and so a large variation between LPM and AWTD numbers is expected.

There are also a number of inherent errors with this method of DSD generation. For example, evaporation and organic growth change the assumed static conditions of the tank, errors in the calibration or acoustic inversion affect the numerical conversion and increased impact velocities due to wind. However, with more development many of these problems can be overcome.

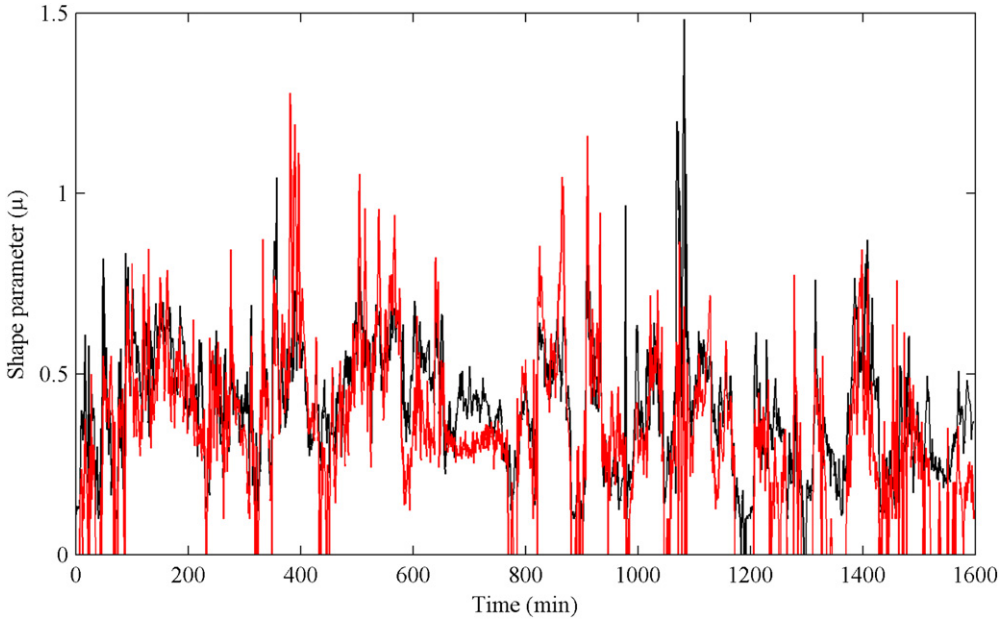

Figure 9. The shape parameter for an exponential fit of the LPM (black) and the AWTD (red) data.

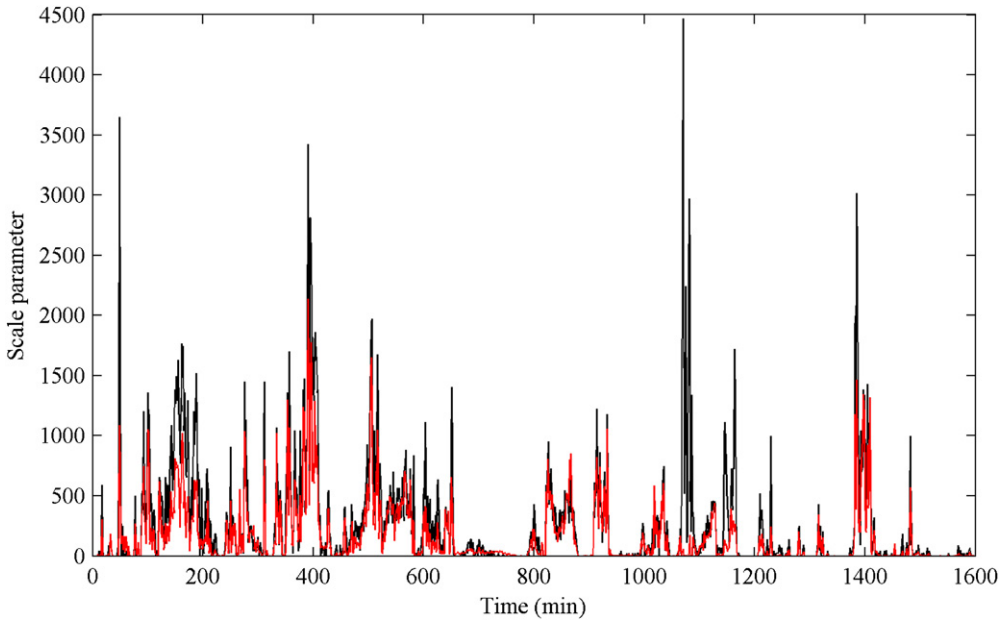

Figure 10. The scale parameter for an exponential fit of all drops over 1.8 mm in diameter for the LPM (black) and AWTD (red).

5. Conclusions

This project has produced a demonstration disdrometer that can measure rain kinetic energy flux density, rain intensity and DSDs with a much greater temporal resolution when compared the LPM (as a direct comparison). Since all other commercial point measurement distrometers use a 60 s integration time and have catchment areas much less than the AWTD, these results can be extrapolated to imply that the AWTD performs better than other commercial alternatives. It can produce rain intensity and kinetic energy flux density information at integration times as low as 1 s with the same standard error. Results have shown that there are large scale variations in these parameters that are not seen with instruments that use a 1 min integration time. These fine-scale variations are likely to become important in the engineering of short, high frequency radio communications links.

The increased catchment area also increases the reliability of the estimation of the large drop-size tail of the DSD. The AWTD uses sophisticated filtering and position algorithms to pick out each individual drop impact on the surface of a liquid. The data are then directly interpreted into a DSD. For drop diameters greater than 1.8 mm the DSD compares well to other commercial alternatives and greatly improves the resolution of the large drop tail of the DSD. For drops less than 1.8 mm the AWTD underestimates the total number of drops. This is because the received impact pressure pulse is below the noise floor of the system and cannot be detected.

Improvements to the amplifiers or hydrophones could resolve smaller drops. This highlights that no single instrument is capable of making a comprehensive observation of the whole DSD; multiple instruments are required.

To facilitate a comparison, temporal analysis was performed by fitting an exponential distribution to both LPM and AWTD derived DSDs with a 1 min integration time. The resultant shape and scale parameters were compared to find that they fitted reasonably well with correlation coefficients of 0.7 and 0.8 respectively and were only degraded by a single erroneous rain event.

The indirect results generate several further questions. Future work should investigate why a multi-parameter model was so well approximated by a single energy estimate. The methodology should be tested upon a test dataset to confirm the high long-term correlation values and provide short-term statistics.

This work also highlights that there are still further enhancements that could be made to other forms of acoustic rain gauges by showing that good estimates of the DSD can be inverted from rainfall intensity data in a mathematically simple way. However, more work is required to formulate a theory that describes the inversion process.

The lack of any very heavy rainfall intensities (the largest was 42 mm h^{-1}) means that the AWTD temporal resolution was never tested to its full potential. Furthermore, the methods used in the direct interpretation mean that the relationship between an impact and the DSD may be too loosely linked, unlike the LPM for example which measures the sizes of the drops directly. However the AWTD compares favourably with another industry standard disdrometer. The current design is a very useful research instrument but its constructional limitations may restrict its widespread adoption. A similar commercial instrument could be developed around a metal plate or tent collector design, which would be considerably cheaper and more resilient than the water tank design. These systems with catchment areas many orders of magnitude larger than current commercial disdrometers, have the potential to develop into disdrometers yielding DSDs with 1 s temporal resolutions.

References

Brodie I and Rosewell C 2007 Theoretical relationships between rainfall intensity and kinetic energy variants associated with stormwater particle washoff *J. Hydrol.* **340** 40–7

COST 210 Management Committee 1991 Influence of the atmosphere on interference between radio communications systems at frequencies above 1 GHz *COST 210* European Commission, Brussels

Deng Q, Anilkumar A V and Wang T G 2007 The role of viscosity and surface tension in bubble entrapment during drop impact onto a deep liquid pool *J. Fluid Mech.* **578** 119–38

Dijk A I J M, Van Bruijnzeel L A and Rosewell C J 2002 Rainfall intensity-kinetic energy relationships: a critical literature appraisal *J. Hydrol.* **261** 1–23

Franz G J 1959 Splashes as a source of sound in liquids *J. Acoust. Soc. Am.* **31** 1080–96

Guo Y P and Williams J E F 1991 A theoretical study on drop impact sound and rain noise *J. Fluid Mech. Digit. Arch.* **227** 345–55

Joss J and Waldvogel A 1967 A raindrop spectrograph with automatic analysis *Pure Appl. Geophys.* **68** 240–6

Kruger A and Krajewski W 2002 Two-dimensional video disdrometer: a description *J. Atmos. Ocean. Technol.* **19** 602–17

Ma B B, Nystuen J A and Lien R J 2005 Prediction of underwater sound levels from rain and wind *J. Acoust. Soc. Am.* **117** 3555–65

Manzello S L and Yang J C 2002 An experimental study of a water droplet impinging on a liquid surface *Exp. Fluids* **32** 580–9

Marshall J S and Palmer W M 1948 The distribution of raindrops with size *J. Atmos. Sci.* **5** 165–6

Medwin H, Kurgan A and Nystuen J A 1990 Impact and bubble sound from raindrops at normal and oblique incidence *J. Acoust. Soc. Am.* **88** 413–8

Medwin H, Nystuen J A, Jacobus P W and Ostwald L H 1992 The anatomy of underwater rain noise *J. Acoust. Soc. Am.* **92** 1613–23

Nystuen J and Amitai E 2003 High temporal resolution of extreme rainfall rate variability and the acoustic classification of rainfall *J. Geophys. Res.* **108** 8378

Nystuen J A 1987 Rainfall measurements using underwater ambient noise *J. Acoust. Soc. Am.* **79** 972–82

Nystuen J A 2001 Listening to raindrops from underwater: an acoustic disdrometer *J. Atmos. Ocean. Technol.* **18** 1640–57

Nystuen J A, McGlothin C C and Cook M S 1993 The underwater sound generated by heavy rainfall *J. Acoust. Soc. Am.* **93** 3169–77

Oguz H N and Prosperetti A 1991 Numerical calculation of the underwater noise of rain *J. Fluid Mech.* **228** 417–42

Ouis D 2005 Modelling the mechanical properties of rubber by means of a five-parameter dispersive model *Proc. Int. Rubber Conf.*

Prosperetti A and Oguz H N 1993 The impact of drops on liquid surfaces and the underwater noise of rain *Annu. Rev. Fluid Mech.* **25** 577–602

Pumphrey H C 1991 Generation of rain noise *Proc. Inst. Acoust.* **13** 192

Pumphrey H C and Crum L A 1989 Underwater sound produced by individual drop impacts and rainfall *J. Acoust. Soc. Am.* **85** 1518–26

Pumphrey H C and Elmore P A 1990 Entrainment of bubbles by drop impacts *J. Fluid Mech.* **220** 539–67

Salles C and Poesen J 2000 Rain properties controlling soil splash detachment *Hydrol. Process.* **14** 271–82

Ulbrich C W 1983 Natural variations in the analytical form of the raindrop size distribution *J. Climate Appl. Meteor.* **22** 1764–75

Winder P N 2010 An acoustic water tank disdrometer *Doctoral Thesis* University of Hull

Winder P N and Paulson K S 2012 The measurement of rain kinetic energy and rain intensity using an acoustic disdrometer *Meas. Sci. Technol.* **23** 015801